Ground Facility Error Analysis and GBAS Performance Evaluation around Suvarnabhumi Airport, Thailand

JIRAPOOM BUDTHO

King Mongkut's Institute of Technology Ladkrabang, Bangkok, 10520, Thailand

PORNCHAI SUPNITHI, Senior Member, IEEE

King Mongkut's Institute of Technology Ladkrabang, Bangkok, 10520, Thailand

NATTAPONG SIANSAWASDI

Aeronautical Radio of Thailand, Bangkok 10120, Thailand

SUSUMU SAITO

Electronic Navigation Research Institute, Tokyo, 182-0012 Japan

APITEP SAEKOW

Faculty of Science and Technology, Stamford University, Bangkok 10520, Thailand

LIN M. M. MYINT

King Mongkut's Institute of Technology Ladkrabang, Bangkok, 10520, Thailand

This work is partially funded by The Royal Golden Jubilee (RGJ) Ph.D. Programme (grant number PHD/0166/2561) and the NSRF via the Program Management Unit for the Human Resources & Institutional Development, Research and Innovation (grant no. B05F640197).

Jirapoom Budtho, Pornchai Supnithi, and Lin M. M. Myint are with School of Engineering, King Mongkut's Institute of Technology Ladkrabang, Bangkok, 10520, Thailand (e-mail: j124p00m@gmail.com, pornchai.su@kmitl.ac.th, and linminmin.my@kmitl.ac.th). Nattapong Siansawasdi is with Air Navigation Radio Aids Department, Aeronautical Radio of Thailand, Bangkok 10120, Thailand (e-mail: nattapong.si@aerothai.co.th). Susumu Saito is with Electronic Navigation Research Institute, National Institute of Maritime, Port and Aviation Technology, Tokyo, 182-0012 Japan (e-mail: susaito@mpat.go.jp). Apitep Saekow is with Faculty of Science and Technology, Stamford University, Bangkok 10520, Thailand (e-mail: apitep.saekow@stamford.edu).
(Corresponding author: Pornchai Supnithi.)

The performances of Ground-Based Augmentation System (GBAS) designed for landing phase of aircraft rely on the accurate characterization of error models. Among various error sources, the multipath model, which is typically constructed by combining environmental errors at airports, must be modeled in GBAS. However, in practice, the multipath effects at a particular airport differ from other airports due to distinct construction sites and continually changing environments, resulting in inaccurate error model in GBAS operations. Therefore, in this work, we develop and evaluate a two-dimensional ground facility error model from the Global Navigation Satellite System (GNSS) stations at the Suvarnabhumi International Airport in Bangkok, Thailand. The results indicate that the elevation and azimuth grid points require around 7 days of observation data to create the GBAS ground facility error model for GBAS operation. The number of observations per day at each elevation and azimuth grid point will determine the data requirements for the complete building of the two-dimensional ground error model. When the proposed model is applied to the GBAS simulation, it is found that the proposed two-dimensional ground error model reduces the root-mean-square deviation (RMSD) of positioning errors by around 0.4 percent to 3.5 percent when compared to the one-dimensional error model and the category B Ground accuracy designator (GAD-B) model, respectively. The maximum vertical protection level (VPL) reduction of the proposed two-dimensional B-value model in comparison with the reference one-dimensional B-value is 0.24 meters, about a 6 percent reduction.

I. INTRODUCTION

En-route and approach segments of the airplane navigation system rely significantly on the Global Navigation Satellite System (GNSS). The ground-based augmentation system (GBAS), an International Civil Aviation Organization (ICAO) standard [1], is intended to assist the aircraft during on and after approach phases of flight [2]; It requires precise coordinates of multiple GNSS reference stations and satellite measurements to compute the pseudorange corrections, which are utilized to enhance the aircraft's positioning and safety.. The safety standard strives to prevent navigational failures and meet integrity requirements. The GBAS performance level, which permits the navigation system and autopilot to assume control of the aircraft until a predetermined decision height, is divided into various categories (CAT). For example, CAT-I is capable of navigating an aircraft to a decision height of 60 meters, whereas for CAT-IIIa, the decision height is reduced to 15 meters.

The Ministry of Internal Affairs and Communications (MIC), and the Ministry of Land, Infrastructure, Transport, and Tourism (MLIT) of Japan have initiated the "GBAS Proof-of-Concept (PoC) Project," a joint technical collaboration between Japan and Thailand [3]. The primary objective of this collaboration project is to install proof-of-concept GBAS equipment at the Suvarnabhumi International Airport and conduct an experiment for the deployment of GBAS in a low geomagnetic latitude region. Since Thailand location is in this area, which is affected by ionospheric irregularities (e.g., equatorial plasma bubble (EPB) and equatorial ionization anomaly (EIA)), an evaluation of its impact is required before

GBAS operations can be approved in Thailand.

In a typical scenario, it is necessary for the computation of the error bound of the pseudorange corrections to take place during the operation of the GBAS. This is accomplished by utilizing approximately three to four reference multi-frequency GNSS stations located within the airport. The computation is based on the most likely errors that could occur within the airport. Ionospheric conditions, tropospheric conditions, and multipath scenarios are the key contributors to unsafe positioning errors that might occur during GBAS operations. As a consequence, it is necessary to estimate and monitor the current positioning errors on both the vertical and lateral axes. They must be kept within a range that is considered acceptable [2].

Multipath is the primary factor to be considered while evaluating the facility errors on the ground. There are three common methods for identifying and eliminating the multipath effects [4] (Chapter 15), [5]: (a) hardware methods from the antenna and receiver, (b) proper location selection before the installation phase, and (c) multipath reduction in pseudorange measurement. From the first two, selecting a suitable survey-grade antenna and installing it in the appropriate area, away from topographical obstructions, is an ideal strategy for multipath reduction, and they are required during the installation process. Furthermore, positioning the antenna directly on the ground reduces the chance of receiving signals reflected from the surface. For the data processing method, previous research has attempted to reduce positioning errors by simulating multipath pseudorange errors from the building's various surfaces and edges [6], [7]. Moreover, the SNR prediction from [8] is employed in an urban region to prevent using misleading observations from low SNR satellites in the position estimation. Based on previous research, geometry screening [9], [10] could be established for the worst-case scenario by excluding up to two satellites from the total number of visible satellites and inflating the sigma values to account for any undetected ionospheric errors in the protection level calculation [11]. Another method for improving positioning is to apply partial elevation masks in some direction to the actual environment of the antenna [12]. When using GPS alone, however, the elimination of a satellite might render the system unusable when they are fewer than the minimal requirements.

Multipath errors at each epoch can be calculated using dual-frequency code and carrier-phase pseudorange measurements in conjunction with the ionosphere-free combination [6]. Since only single-frequency measurements are obtained from the GBAS reference stations, the multipath errors cannot be directly computed. Fortunately, the multipath is a component of the ground facility error. This ground facility error can be computed using a single frequency measurement referred to as the B-value. In [13], [14], the B-value is the consistency checking parameter of the pseudorange corrections from all reference stations, which is then used to calculate the multipath errors. In order to compute the B-values, the precisely estimated positions of all GBAS reference stations are required. Then, as a function of elevation angle, a model of ground facility error based on B-value is created.

The conventional ground facility error is created by combining environmental errors from a variety of various airports. However, the environments of some airports have a significant impact on GBAS operations differently. As a result, empirical pseudorange error and ionospheric model may differ from that specified in the GBAS standard. Furthermore, various ground facility error characteristics may result from the extended phase of airport construction. Due to multipath error from such sites as well as the ionospheric model, the protection level in GBAS operations can be either over bounded or under bounded, resulting in excessive conservatism or potential loss of integrity, respectively. Precise ground facility and ionospheric error models for each airport are required to enhance the performances of the GBAS.

As a result, we propose a two-dimensional ground facility error model (from B-value) as a function of elevation and azimuth angles. This model is based on the empirical data from the GNSS stations in the Suvarnabhumi International airport area. To analyze performance, the VPL simulation from the proposed models and the reference GBAS model are compared to the empirical positioning error. This comparison is accomplished using the root-mean-square error (RMSE). In order to evaluate whether there has been a performance improvement or not, the GBAS simulation will make use of the reference GBAS model, our ground facility error model, and an ionospheric model. The following is a breakdown of how this article is structured. In Section 2, we overview the pseudorange correction and B-value estimation in GBAS standard. The protection level calculation in GBAS is also described in this Section. The experimental setup and the related parameters in GBAS simulation are explained in Section 3. The simulation results are discussed in Section 4. In the final Section, we make the conclusions.

II. METHODOLOGY

A. Pseudorange correction in GNSS signals

In GBAS, the smoothed code pseudorange measurement, $\hat{R}^s(t)$, is computed by smoothing the noisy (but unambiguous) code pseudorange data with precise (but ambiguous) carrier phase measurements. In [15], a Hatch filter method is used for each satellite (s) with a 100-second smoothing time constant (n = 100) as follows:

$$\hat{R}^s(t) = \frac{1}{n}R(t) + \frac{n-1}{n}\left[\hat{R}^s(t-1) + \left(\Phi(t) - \Phi(t-1)\right)\right], \tag{1}$$

where $R(t)$ and $\Phi(t)$ are the code and carrier phase pseudorange at time t.

The true range $\left(Tr_m^s\right)$ is calculated using the precise locations of the receiver (m) and each satellite (s). From the base station, the smoothed code pseudorange will be compared to the true range for each satellite's corrected parameters. Then, the pseudorange corrections, $\rho_{c,m}^{s}(t)$, at t epoch of each station can be estimated from

$$\rho_{c,m}^{s}(t) = \hat{R}_{m}^{s}(t) - Tr_{m}^{s}(t) + \tau_{m}^{s}(t), \tag{2}$$

where τ_{m}^{s} is the satellite clock offset.

The calculated pseudorange correction obtained from (2) contains the receiver clock offset. On the other hand, for receiver m, all satellite pseudorange corrections experience the same receiver clock offset. This receiver clock offset can be uniformly removed from the pseudorange correction, and this constant offset may be estimated by a weighted average of pseudorange corrections from all satellites, i.e.,

$$\rho_{sc,m}^{s}(t) = \rho_{c,m}^{s}(t) - \frac{1}{N}\sum_{s\subset S_c} k^{s}\rho_{c,m}^{s}(t), \tag{3}$$

where N and S_c represent the total number and subset of satellites that can be monitored by all receivers at time t, respectively and k is the weighting factor; $\sum_{s\subset S_c} k^{s} = 1$. The weight factor k used here is the sine of the satellite elevation angle. Afterward, before transmitting the averaged pseudorange corrections from all GNSS receivers from (3), it is necessary to monitor the pseudorange corrections without receiver clock offsets, $\rho_{sc,m}^{s}(t)$. The B-value is utilized in GBAS to monitor the potential failure of a single reference receiver, including environmental factors such as multipath. Monitoring the mean value of pseudorange corrections is the task of other GBAS integrity monitors.

Prior to the GBAS processing unit broadcasting the pseudorange correction, it is essential that the pseudorange corrections adjusted by each reference station are consistent. The B-value calculation is used to compare the current residual error of the pseudorange error to a predetermined threshold. The B-value, B_{m}^{s}, for the m^{th} station with respect to the s^{th} satellite is calculated using the following formula:

$$B_{m}^{s} = \frac{1}{M}\sum_{i=1}^{M}\rho_{sc,i}^{s} - \frac{1}{M-1}\sum_{i=1,i\neq m}^{M}\rho_{sc,i}^{s}, \tag{4}$$

where M is the number of GNSS reference receivers. In addition, if the B-value from any reference station exceeds the threshold, the pseudorange correction for the related reference station is removed from the broadcast pseudorange corrections.

B. Error models in GBAS

1). GBAS residual error model

Integrity, accuracy, continuity, and availability must all be kept within allowable levels in GBAS. The GBAS error model, which includes ground facility error, aircraft facility error, tropospheric error, and ionospheric error, can be used to calculate the statistical residual errors in the system. Uncorrelated zero-mean Gaussian random variables are considered to be the basis of these errors. The GBAS residual error model is computed from [16],

$$\sigma^{2}(t) = \sigma_{pr\_gnd}^{2}(t) + \sigma_{pr\_air}^{2}(t) + \sigma_{tropo}^{2}(t) + \sigma_{iono}^{2}(t), \tag{5}$$

where $\sigma_{pr\_gnd}^{2}, \sigma_{pr\_air}^{2}, \sigma_{tropo}^{2}$, and σ_{iono}^{2} are the standard deviation from the ground facility, aircraft facility, troposphere, and ionosphere, respectively. In [16], the σ_{tropo}^{2} and σ_{air}^{2} are calculated from the GBAS standard model as a function of the satellite's elevation angle. The σ_{iono} and σ_{pr_gnd}, on the other hand, are related to the airport's local environment and require pre-analysis from observation data in the GBAS installation area. The development of both models will be covered in the following section.

2). Current ground facility error model and the proposed GBAS two-dimensional ground facility error model

The current ground facility error value, σ_{pr_gnd}, can be applied to GBAS using either the ground accuracy designator (GAD) model or the B-value model [16]. For the GAD model, the σ_{pr_gnd} can be calculated from

$$\sigma_{pr\_gnd}^{2} = \frac{\left(a_0 + a_1 e^{-E/\theta_0}\right)^{2}}{M} + \left(a_2\right)^{2}, \tag{6}$$

where E is the elevation angle (degrees), and a_0, a_1, a_2 and θ_0 are parameters that are defined based on the GAD category and the GBAS Approach Service Type (GAST), which are determined by the type of GNSS antenna and receiver installed at each airport. For example, if GAD-B for the GAST-C service [16] is selected, $a_0 = 0.16$ meters, $a_1 = 1.07$ meters, $a_2 = 0.08$ meters, and $\theta_0 = 15.5$ degrees, respectively. This example is the scenario for GBAS operating without the benefit of multipath limiting GNSS antennas, only high performance GNSS receivers with geodetic-grade antennas are considered. For the B-value model, based on the B-values computed from (4), which is used to indicate the uncertainties in pseudorange correction in GBAS, σ_{pr_gnd} can also be computed from a one-dimensional B-value model [2] in one-dimensional function, i.e.,

$$\sigma_{pr\_gnd}(E) = \sqrt{\sigma_{B}^{2}(E) * (P(E) - 1)}, \tag{7}$$

where

$$\sigma_{B}^{2}(E) = \frac{1}{P(E)}\sum_{j=1}^{P(E)}\left(B_j(E) - \overline{B(E)}\right)^{2}, \tag{8}$$

E is the elevation angle range to be considered, and P is the number of B-values in these elevation angle range.

To demonstrate both current GAD and B-value to be used for σ_{pr_gnd} computation, a one-dimensional plot based on elevation angle is shown in Fig. 1. The x-axis is the elevation angle, whereas the y-axis is σ_{pr_gnd} to be used in the GBAS error model. In this figure, the GNSS stations at Suvarnabhumi airport are used to create the B-value model.

This article has been accepted for publication in IEEE Transactions on Aerospace and Electronic Systems. This is the author's version which has not been fully edited and content may change prior to final publication. Citation information: DOI 10.1109/TAES.2023.3326134

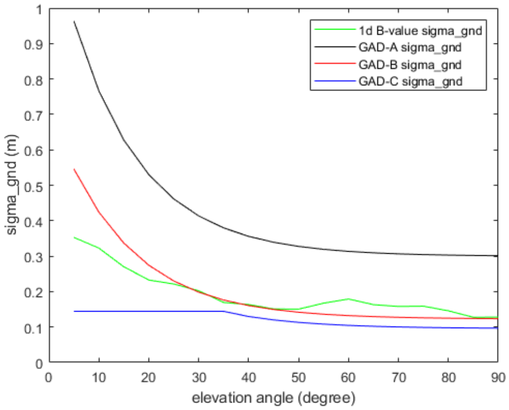

Fig. 1. **One-dimensional σ_{pr_gnd} computed from GAD-A, GAD-B, GAD-C, and B-value models.**

According to Fig. 1, the one-dimensional B-value model generates σ_{pr_gnd} that is closely related to the GAD-B model. However, there are segments of the elevation angles where the σ_{pr_gnd} from the B-value model is approximately 0.1 to 0.2 meters higher than the GAD-B model. This provides the evidence that in the same elevation angle range, σ_{pr_gnd} from the different azimuth angles could provide the different characteristics. Therefore, in this work, the two-dimensional B-value model is introduced. The σ_{pr_gnd} computation from (7) is revised, i.e.,

$$\sigma_{pr\_gnd}(\alpha, E) = \sqrt{\sigma_B^2(\alpha, E) * (P(\alpha, E) - 1)}, \qquad (9)$$

where

$$\sigma_B^2(\alpha, E) = \frac{1}{P(\alpha, E)} \sum_{j=1}^{P(\alpha,E)} \left(B_j(\alpha, E) - \overline{B(\alpha, E)} \right)^2, \qquad (10)$$

α is the azimuth angle grid point to be considered, E is the elevation angle grid point to be considered, and P is the number of B-values in the azimuth and elevation angle range. In order to facilitate comprehension, Fig. 2 depicts the σ_{pr_gnd} grid based on a two-dimensional B-value model.

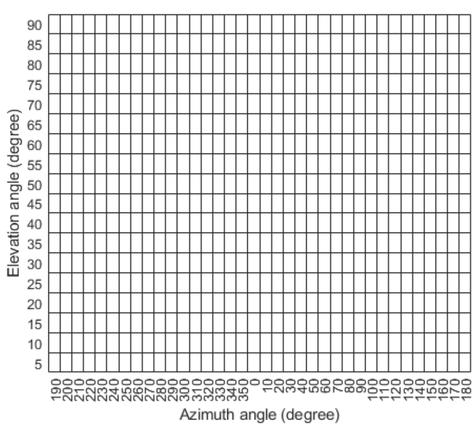

Fig. 2. **The proposed two-dimensional σ_{pr_gnd} grid computed from B-values.**

After creating the σ_{pr_gnd} value from two-dimensional B-value model, it will be supplied to the aircraft positioning system as a part of the pseudorange uncertainty [2]. In addition, protection levels are computed in GBAS simulation at the aircraft using σ_{pr_gnd} derived from the GAD model and the one- and two-dimensional B-value models.

3). GBAS ionospheric model with near real-time vertical ionospheric delay gradient statistic

In GBAS model, the error caused by ionospheric effect is computed from

$$\sigma_{iono} == F_{pp} \cdot \sigma_{VIG} \cdot (x_{air} + 2 \cdot \tau \cdot v_{air}), \qquad (11)$$

where F_{pp} is the slant factor, σ_{VIG} is the standard deviation of the vertical ionospheric delay gradient (m/m), x_{air} is the distance between aircraft and airport (m), τ is a constant depending on the service type (GBAS approach service type: GAST), and v_{air} is the aircraft horizontal approach velocity (m/s).

The GBAS standard requires the use of σ_{VIG} among other parameters to assess the vertical and lateral protection levels (VPL and LPL). When this parameter (often a constant) is applied to various ionospheric conditions, both over- and under-estimation of the positioning errors may occur. As a result, near real-time σ_{VIG} values from each satellite utilized in the GBAS analysis is chosen to improve the protection levels to be as close as possible to the actual positioning error. Each satellite's σ_{VIG} is calculated independently using the ionospheric delay gradients from the day before. This gradient is computed using a single frequency method [17], [18]. The ratio test is used to validate the gradient reliability. This article will compare the root mean square error of the protection levels between the GBAS model and the proposed model.

C. Protection level in GBAS

Using a navigation performance indicator known as protection level (PL), the GBAS needs to set a limit on the amount of positioning uncertainty that is acceptable for the aircraft. In the GBAS standard [16], [19], [20], PL are used to certify the availability, accuracy, integrity, and continuity of the GBAS. The idea behind PL is to generate a bound of acceptable errors by using real-time errors measured from the system. When the protection level is smaller than the alert limit (AL), GBAS service will become available. Vertical and lateral protection levels are distinguished by the PLs' distinction (VPL and LPL). For the purpose of computing the PL in the null hypothesis, H0, which PLs are determined assuming that there is no malfunction in the reference receiver, the following equations are utilized:

$$VPL_{H0} = K_{ffmd} \sigma_{vert} \qquad (12)$$

and

$$LPL_{H0} = K_{ffmd} \sigma_{lat}, \qquad (13)$$

This article has been accepted for publication in IEEE Transactions on Aerospace and Electronic Systems. This is the author's version which has not been fully edited and content may change prior to final publication. Citation information: DOI 10.1109/TAES.2023.3326134

where the VPL_{H0} and LPL_{H0} protection levels refer to the vertical and lateral protection levels, respectively, under the fault-free hypothesis. The K_{ffmd} probability of fault-free missed detection is used to calculate the multiplier for the vertical and lateral standard deviation. σ_{vert} and σ_{lat} represent the standard deviation of residual errors in the vertical and lateral directions, respectively. These two sigmas are derived from the GBAS error model in (5) via the formula:

$$\sigma_{vert} = \sqrt{\sum_{i=1}^{N} s_{vert,i}^2 \, \sigma_i^2} \tag{14}$$

and

$$\sigma_{lat} = \sqrt{\sum_{i=1}^{N} s_{lat,i}^2 \, \sigma_i^2}\ , \tag{15}$$

where S_{vert} and S_{lat} are the elements in the projection matrix [16] that are being used to transform the standard deviation from range domain to position domain.

D. Geometry screening in GBAS

Since the aircraft's satellite receiver may be inferior to that of the ground station, the aircraft may receive a fewer number of satellites. Therefore, we simulate the protection level separately from the aircraft including 1 and 2 possible cases of satellite loss [9], which is $\sum_{k=N-2}^{N} \binom{N}{k}$ cases, where N is the number of visible satellites at each epoch.

In the position domain, ionosphere-induced range errors, also known as ionospheric delay, can be monitored at the GBAS reference ground station. However, there is a possibility that the largest possible vertical position error could occur without being detected by the ionospheric monitoring. Therefore, the maximum ionospheric-induced range errors error in vertical (MIEV) is required in addition to the calculation of the protection level. The MIEV is derived from the ionospheric-induced range errors in vertical (IEV), i.e.,

$$\text{IEV}_{k1,k2} = \left|S_{\text{vert},k1}\varepsilon_{k1}\right| + \left|S_{\text{vert},k2}\varepsilon_{k2}\right|, \tag{16}$$

where S_{vert} is the vertical position component of the projection matrix as described in (14) and ε is the ionospheric-induced range errors for satellite $k1$ and $k2$.

When using the tolerable error limit (TEL) as a threshold [10], the MIEV computation is used to inflate the σ_{VIG} value until all the unavailable MIEV satellite geometry subsets are in the unavailable protection level subsets. Then, the updated σ_{VIG} will be transmitted with the others to each aircraft for the calculation of its protection level. In this simulation, the ground geometry screening is implemented based on the vertical Category I tolerable error limit determined by the U.S. Federal Aviation Administration (FAA), which is 28.078 m. (at the minimum decision height of 200 ft) [10], [11].

III. EXPERIMENTAL SETUP

In this work, by utilizing GPS data from the GBAS reference stations, we investigate the ground facility errors in Suvarnabhumi International Airport, Thailand. The stations AER1 AER2, and AER3 are used as the GBAS reference stations as shown in Fig. 3. The station coordinates were calculated using 32 GPS satellites over the duration of one day using precise point positioning (PPP) [21], [22]. For this GBAS error model analysis and simulation, the days from 1 to 100 in 2019 in dry season are chosen because the ground reflectivity index is lower during this season than during the rainy season, reducing the multipath effect. For GNSS separation distance in GBAS setup, since the GBAS can operate while one of the reference stations becomes unavailable, a separation distance of 2 to 5 kilometers is chosen to reduce the possibility of all reference stations being simultaneously affected by a single GNSS jammer. According to previous research, some types of GNSS jammer coverage can extend up to 9 kilometers [23], [24]. If all GBAS reference stations are within jammer coverage due to the standard separation distance configuration (200 meters), the GBAS will become inoperable. As a result, 2 to 5 kilometers are chosen to analyze the protection levels in longer separation distances.

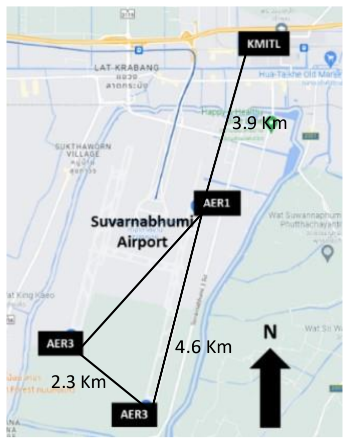

Fig. 3. **The GNSS stations (AER1, AER2, and AER3) of GBAS which are located in Suvarnabhumi International Airport, Thailand.**

We obtain the pseudorange corrections at each time from 3 stations from Suvarnabhumi International Airport, and then the B-value from each station is used for the consistency check of the correction. Next, the one-day B-value data will be evaluated to identify the minimal data duration necessary for the creation of the two-dimensional σ_{pr_gnd} model. In addition, the cumulative availability of the σ_{pr_gnd} model will be investigated in order to determine the percentage of the ground facility error model for data ranging from 1 to 100 days.

For the two-dimensional σ_{pr_gnd} model, the grids with azimuth angle resolutions of 10 degrees and elevation angle of 5 degrees are created. In GBAS simulations, the KMITL station coordinate, as shown in Fig. 3, is used to estimated positioning errors. This station is located on the roof of the tallest building within a 20-kilometer radius of the airport, beneath the landing path for runway 19L. In addition, the one- and two-dimensional σ_{pr_gnd} model will be used to simulate the protection levels. For the calculation of positioning error, the distance between positions estimated by PPP and GBAS pseudorange correction was used. According to analysis in [25], stationary phase positioning errors fall within the same range as approach and landing phase positioning errors. Additional errors are unaffected by the moving antenna [26]. This study primarily focuses on the GBAS simulation based on the stationary PE results. Additionally, when evaluating the GBAS performance, for the ionospheric model, GBAS uses the pre-processed ionospheric delay gradient from previous work [17]. In addition, to isolate the impact of ground facility errors from high ionospheric disturbance in the simulation, data from DOY 001 in 2019 is selected as the simulation example, as there was no high ionospheric disturbance on this day.

IV. RESULTS AND DISCUSSIONS

A. Number of day requirement for the ground facility error model in GBAS

For the creation of σ_{pr_gnd} at each azimuth and elevation angle model in the grid form, the B-values at those grid points are required over specific time periods. However, the B-value derived from one day of data may not suffice for this computation. Data from a short period of time might not accurately represent the σ_{pr_gnd}, leading to an overestimation or underestimation of the protection levels. On the other hand, if the airport's multipath changes, data over a long-time span will delay the updated model. For the creation of a suitable error model, convergence time analysis is required. 100 days of GNSS data, which contains 916623 samples of B-values, are used to verify the convergence period of the sigma creation from B-values in order to determine the amount of data required. Based on the azimuth and elevation grid resolution mentioned in section II, 648 combinations of grid points are required. Five grid point examples are plotted in time series to illustrate the convergence time in different cases in Fig. 4.

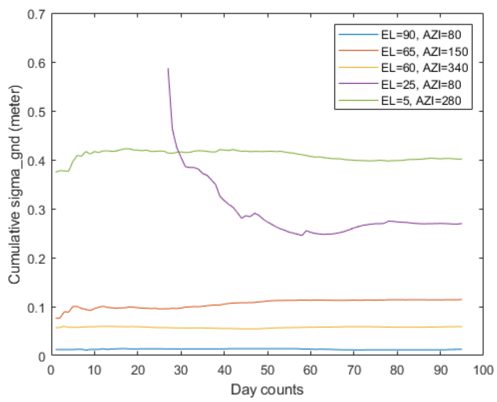

Fig. 4. **The σ_{pr_gnd} from each elevation and azimuth angle grid from 100 days at Suvarnabhumi Airport GBAS station in 2019.**

In Fig. 4, the σ_{pr_gnd} values are larger at low elevation angles, as expected by the estimated errors of the ground facility [5] due to the multipath effect. The cumulative σ_{pr_gnd} for the convergence time analysis indicates that ten days of B-value data are sufficient for the convergence in most cases. However, at the elevation of 25 degrees and azimuth of 80 degrees (purple line in Fig. 4), up to 45 days of B-value observations are necessary because the satellites only started to be visible at this direction on DOY 28. In addition, because the quantity of observation data is fewer than in other grid points, approximately 17 days of observation in this grid point are required for convergence. Therefore, the number of observations per day at each elevation and azimuth grid point determines the data requirements for the σ_{pr_gnd} model.

Based on previous work, certain grid points of elevation and azimuth angle require more data than the others for the σ_{pr_gnd} convergence time. Therefore, all grid points will be analyzed for the convergence time. The histogram from the convergence result is plotted from the 648 possible elevation and azimuth grid points as shown in Fig. 5. Convergence is considered to have occurred when the updated σ_{pr_gnd} is less than 0.005 meters different from the previous one or less than a 1 percent change of the maximum σ_{pr_gnd}.

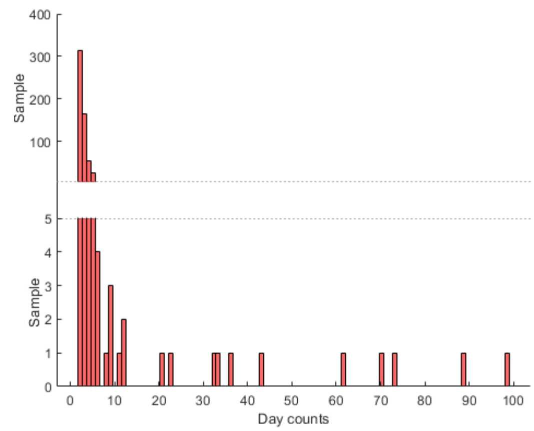

Fig. 5. **The histogram from the convergence time of σ_{pr_gnd} from the 648 possible elevation and azimuth grid points.**

According to the convergence time result, approximately 567 combinations of the elevation and azimuth grid points require around 7 days of observation data for the creation of σ_{pr_gnd} model. Only 11 grid points require more than 10 days depending on when the first observation can be received. Please note that there are 64 grid points lack sufficient observation data to create the σ_{pr_gnd} model within 100 days, some missing grid points can be easily filled by using the interpolation from the nearby grid points excluding the area not suitable for a simple interpolation. The introduced two-dimensional plot will be used to explain how to utilize data from the missing part again in Fig. 9. Next, since percentages of the σ_{pr_gnd} availability are required for the GBAS analysis, the cumulative availability percentages of the σ_{pr_gnd} from all elevation and azimuth

This article has been accepted for publication in IEEE Transactions on Aerospace and Electronic Systems. This is the author's version which has not been fully edited and content may change prior to final publication. Citation information: DOI 10.1109/TAES.2023.3326134

angles is shown in Fig. 6. The x-axis is the day counts for the σ_{pr_gnd} model availability from all possible elevation and azimuth angle grid points.

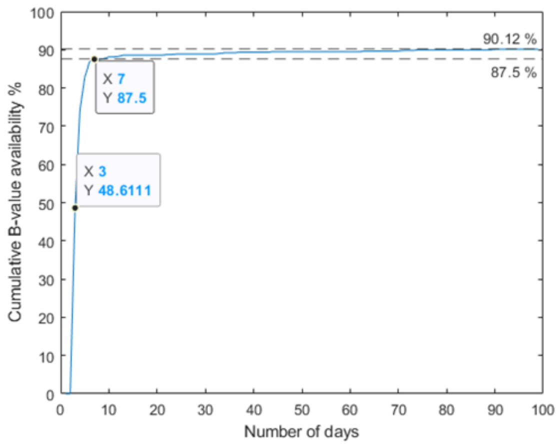

Fig. 6. The cumulative count of the percentage of σ_{pr_gnd} availability based on the sum of observation data ranging from 1 to 100 days.

From the results, there is no σ_{pr_gnd} availability until the third day, which corresponds to approximately 50 percent or 324 of 648 combinations of all possible elevation and azimuth grid points. On day seven, the availability of σ_{pr_gnd} increases to 85.7 percents or 567 of 648 combinations, sufficient for the GBAS simulation. The following 10-day results provide small increment percentages. Since the satellite footprints from the preceding 10 days are nearly identical, small variations from day-to-day data are observed. Although more than 100 days of observation are used to create the σ_{pr_gnd} model, the availability is only increased by about 2 percent or 9 more combinations of 648 total grid points. Please note that, we have tried other grid resolution such as 5 degrees, however, the maximum cumulative availability decreases from 90.12 to 82.71 percent, or 1057 of 1278 possible combinations. Therefore, 10 degrees grid resolution of azimuth is selected in the GBAS error model.

B. Skyplot of in the Suvarnabhumi Airport area

The computed σ_{pr_gnd} values of the grid-formatted data are shown in Fig. 7 to visualize the two-dimensional multipath plots based on the B-value computation in (9). The azimuth angle is represented by the x-axis, while the elevation angle is represented by the y-axis. Each color corresponds to a different σ_{pr_gnd} value. The resolutions of the elevation and azimuth angle grids are 5 and 10 degrees, respectively. Then, based on (7), B-values data is utilized to estimate one-dimensional σ_{pr_gnd} as shown in Fig. 8, and compared to the existing GAD-B model in GBAS. Furthermore, Fig. 9 shows how the grid-formatted data is used to generate the skyplot, which displays a circular graph similar to how satellites appear in the sky. The azimuth angles in the skyplot are rotated clockwise. The elevation angle is indicated by the circle. The outside ring represents the lower elevation beginning at 0 degrees, while the center of the circle represents an elevation angle of 90 degrees. The different colors represent the σ_{pr_gnd} strengths, similar to the grid-formatted data in Fig. 7, with dark blue representing approximately 0.1 meters and pink representing approximately 0.5 meters.

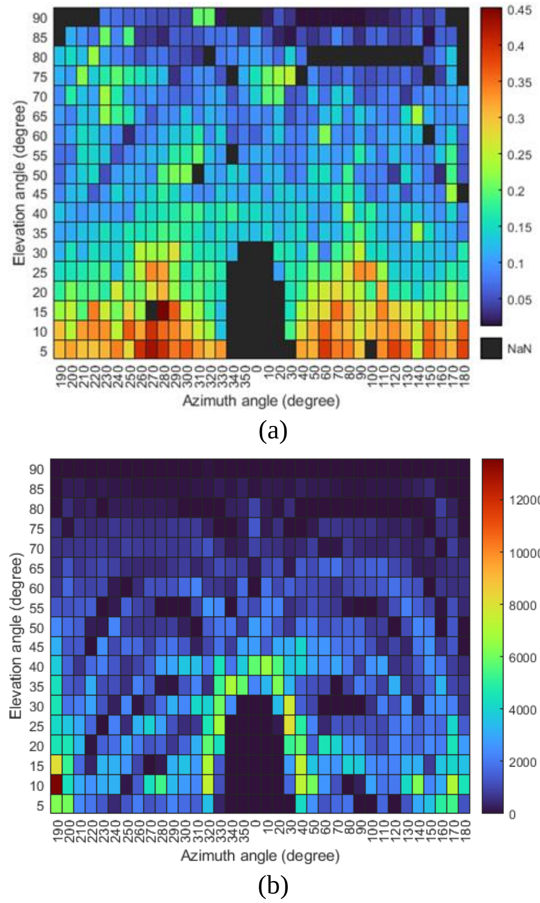

Fig. 7. (a) 2-dimensional σ_{pr_gnd} diagram from the Suvarnabhumi Airport GBAS station and (b) the number of data points corresponding to each grid point in (a).

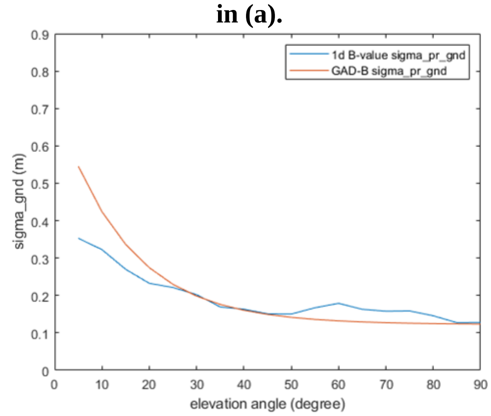

Fig. 8. The comparison of σ_{pr_gnd} from the Suvarnabhumi Airport GBAS station between the reference GAD-B model and the one-dimensional model estimated from B-values.

This article has been accepted for publication in IEEE Transactions on Aerospace and Electronic Systems. This is the author's version which has not been fully edited and content may change prior to final publication. Citation information: DOI 10.1109/TAES.2023.3326134

Using the one-dimensional analysis as shown in Fig. 8, the reference GBAS GAD-B model generates σ_{pr_gnd} with a comparable trend to that of the B-value model at the elevation angles higher than 25 degrees. On the other hand, the reference one-dimensional B-value model provides a 0.1 to 0.2 meters lower σ_{pr_gnd} than GAD-B at the elevation angles of less than 20 degrees. The results demonstrate that the ground facility errors of the GAD-B model are overestimated at low elevation angles when the GBAS reference stations are equipped with geodetic-grade GNSS antennas in this location. However, at around 60 to 75 degrees elevation angles, it can be seen from the skyplot result, in Fig. 9, that azimuth angles between 220 and 250 have a sigma value that is twice as high as other azimuth angles. Therefore, the overall σ_{pr_gnd} values of the one-dimensional B-value model at the elevation angles between 60 and 75 degrees are increased by 0.1 to 0.3 meters.

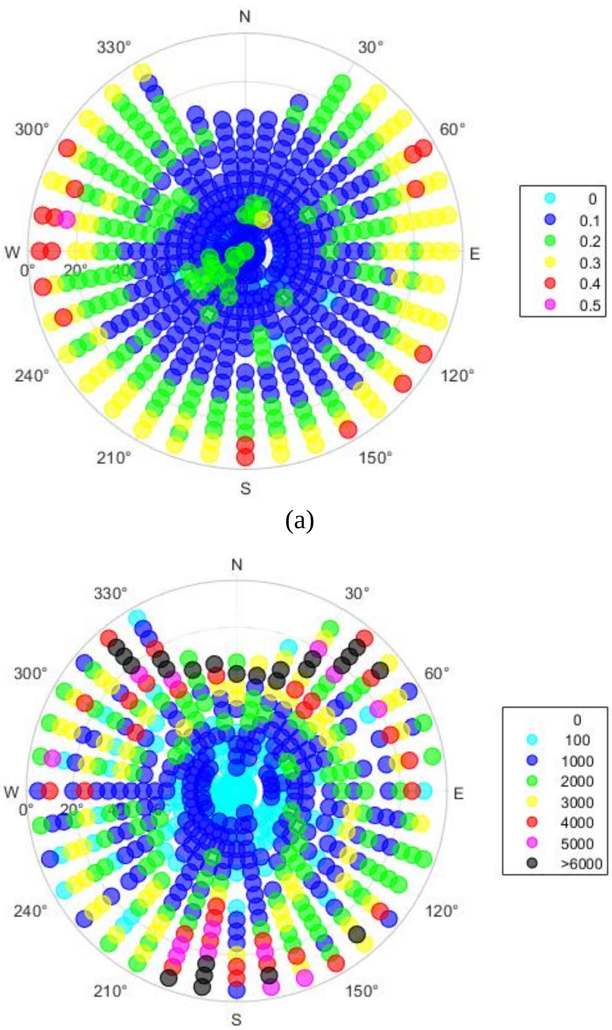

(a)

(b)

Fig. 9. **(a) 2-dimensional σ_{pr_gnd} skyplot from the Suvarnabhumi Airport GBAS station and (b) the number of data points corresponding to each point in skyplot (a).**

From the two-dimensional analysis of the σ_{pr_gnd} results in Fig. 9, when examined at the same low elevation angle, the results of the grid and the skyplot indicate that some azimuths, for example, on the Western side, have twice as high σ_{pr_gnd} values as others. Increasing ground facility errors at approximately 290-degree azimuth are also observed. When compared at higher elevation angle, the σ_{pr_gnd} are mostly less than 0.2 meters. Moreover, it is clearly seen that the Southeast side shows significantly low σ_{pr_gnd}. For elevation angles higher than 20 degrees, the values are less than 0.1 meters. This result indicates that the multipath characteristics of various regions are not identical. Additionally, there is no visible satellite with an elevation angle of less than 30 degrees in the northern hemisphere. Due to the nature of the satellite constellation footprints and the airport location in the northern hemisphere, 13.7 degrees or about 1,500 kilometers from the equator, the satellites cannot be seen in the northern hemisphere on the skyplot, resulting in a grid gap. However, this occurrence will have practically no effects on the GBAS simulation, as all satellites observed on the next day will have nearly identical motion traces to the previous day. Therefore, the missing data in grid gap does not affect the GBAS simulation.

C. Protection level comparison between the GBAS model, multipath model, and the ionospheric model with the positioning errors

During a GBAS operation, only PLs can be computed onboard relying on GPS geometry, but PE cannot be computed onboard. Consequently, in this work, since the KMITL station coordinate is known, therefore, we can estimate the actual positioning error (PE). Basically, to obtain PE, on the purpose of comparison with PL, we assume the receiver at KMITL station is regarded as the assumed aircraft in GBAS simulations. To assess the performances of the new two-dimensional ground error model estimated from B-values, the vertical protection levels derived from each model will be compared to the actual PE. Initially, the GBAS simulation will be conducted from 11:00 to 13:00 UTC in Fig. 10 to observe the highest improvement of the VPL simulation from the proposed B-value model to the GAD-B model. In addition, the satellite constellation and σ_{pr_gnd} from each satellite at approximately 12:00 UTC, which is the lowest level of protection for DOY 001 in 2019, will be depicted in the same figure. Next, Fig. 11 depicts a day's duration of GBAS simulation on the same day. Each model's root-mean-square deviation (RMSD), when PLs are compared to the reference PEs, is presented in Table 1.

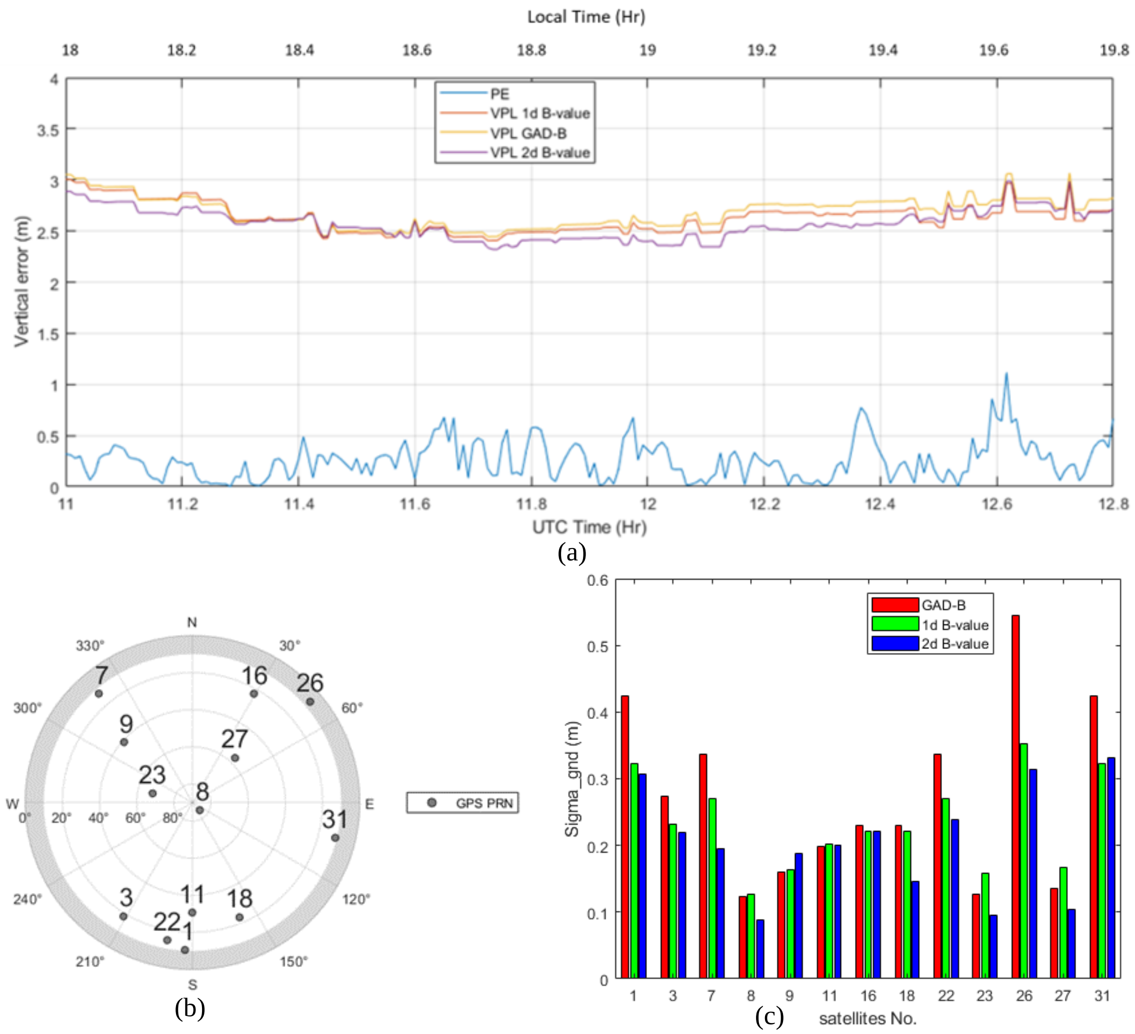

Fig. 10. **(a) Positioning error (PE) and simulation of protection levels from the reference one-dimensional models and the proposed two-dimensional model estimated based on the B-value at approximately 12:00 UTC., (b) the satellite constellation at second of day 43,200, and (c) the σ_{pr_gnd} of satellites between each model.**

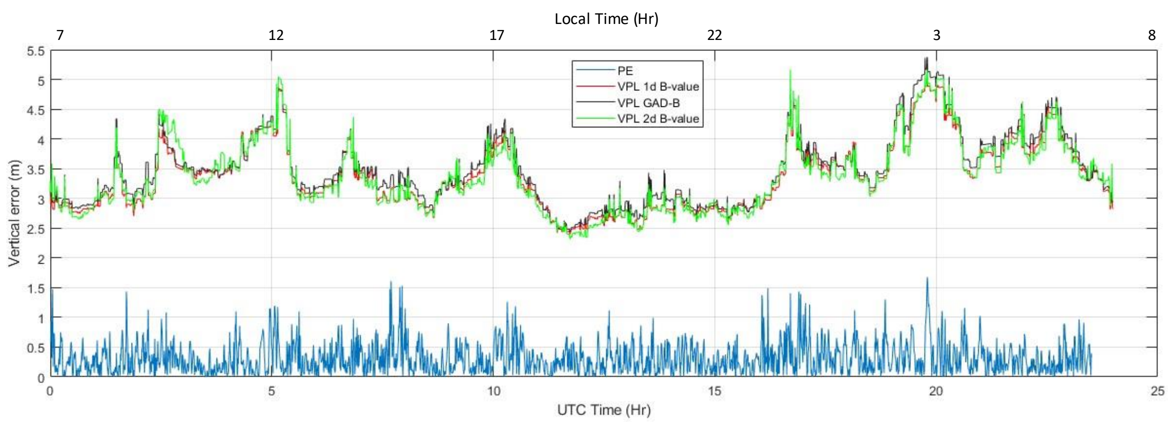

Fig. 11. **The positioning error (PE) and simulation of protection levels from the reference one-dimensional models and the proposed two-dimensional model estimated based on the B-value on DOY 001 in 2019.**

Fig. 10 depicts the protection levels at approximately 12:00 UTC from the reference one-dimensional ground facility error models (GAD-B and B-value) and the proposed two-dimensional B-value ground facility error model. When we consider the satellite geometry at the second of day (SOC) 43200 as shown in Fig. 10b, the elevation angles of PRN 01, 03, 07, 22, 26, and 31 are less than 30 degrees. As a result, when the one-dimensional B-value model is applied, the σ_{pr_gnd} values from these satellites are reduced by approximately 0.1 meters compared to the reference GAD-B model, as shown in Fig. 10c. Moreover, compared to both reference models, the proposed two-dimensional B-value model (blue bar) provides the largest reduction in σ_{pr_gnd} values. Next, when protection level is considered, in Fig. 10a, the VPL at 12:00 UTC for the GAD-B model is 2.6 meters. VPL is reduced to 2.5 meters using the one-dimensional B-value model and to 2.4 meters using the proposed two-dimensional B-value model, which is 7.69 percent less than the GAD-B model. Based on one-day VPL simulation in Fig. 11, the maximum VPL reduction from the reference one-dimensional B-value to the proposed two-dimensional B-value model is 0.24 meters at 07:13:37 UTC (from 3.90 to 3.66 meters), which corresponds to a 6.15 percent reduction in VPL.

TABLE 1.
The GBAS simulation and the RMSD comparison between each ground error model to the positioning error (PE).

Error model	RMSD computed with the positioning errors (meters)
GAD-B	3.2269
One-dimensional σ_{pr_gnd} model	3.1248
Two-dimensional σ_{pr_gnd} model	3.1132

In comparison to positioning errors (PE), the reference GBAS error model (GAD-B) generates the highest protection levels. At approximately 4:00 a.m. UTC, as shown in Fig. 11, the two-dimensional σ_{pr_gnd} model has a significantly lower VPL than the other models. The overall σ_{pr_gnd} values from the one-dimensional B-value model are larger than those from the two-dimensional model because they are derived from the average of each azimuth angle. According to a one-day GBAS simulation in Table 1, the GAD-B model's RMSD is 3.2269 meters. The one-dimensional sigma model reduces the RMSD to 3.1248 meters, while the two-dimensional σ_{pr_gnd} model reduces it to 3.1132 meters, 0.4 percent less than the one-dimensional model, and 3.5 percent less than the GAD-B model.

V. CONCLUSIONS

In this work, a more precise two-dimensional ground facility error model is developed by using B-values from low-latitude GNSS stations. From the convergence time analysis in the creation of ground error model, the results indicate that at least seven days of B-value data are needed to achieve convergence. From the skyplot of σ_{pr_gnd} analysis, the proposed two-dimensional B-value model provides the highest reduction in σ_{pr_gnd} of approximately 20 percent compared to the reference one-dimensional models. In the GBAS simulation, the maximum VPL reduction of the proposed two-dimensional B-value model is about 6 percent when compared with the reference one-dimensional B-value. The proposed model can be implemented to the existing GBAS reference stations with the hardware pre-analysis procedure, and the error model can be updated based on current environmental conditions. Future work could also include an extension to multi-constellation GNSS for GBAS.

ACKNOWLEDGMENTS

This work is partially funded by The Royal Golden Jubilee (RGJ) Ph.D. Programme (grant number PHD/0166/2561) and from the NSRF via the Program Management Unit for the Human Resources & Institutional Development, Research, and Innovation (grant no. B05F640197).

REFERENCES

[1] ICAO, "Guide for Ground Based Augmentation System implementation," 2013.

[2] E.-114A EUROCAE, "MOPS for global navigation satellite ground based augmentation system ground equipment to support category I operations," 2013.

[3] ICAO, "GBAS Proof-of-Concept Project," in *The third meeting of GBAS-SBAS Implementation Task Force (GBAS-SBAS ITF/3)*, Video conference, Sep. 2021.

[4] *Springer Handbook of Global Navigation Satellite Systems*. 2017. doi: 10.1007/978-3-319-42928-1.

[5] D. Prochniewicz and M. Grzymala, "Analysis of the impact of multipath on Galileo system measurements," *Remote Sens (Basel)*, vol. 13, no. 12, 2021, doi: 10.3390/rs13122295.

[6] L. Lau and P. Cross, "Development and testing of a new ray-tracing approach to GNSS carrier-phase multipath modelling," *J Geod*, vol. 81, no. 11, 2007, doi: 10.1007/s00190-007-0139-z.

[7] S. H. Byun, G. A. Hajj, and L. E. Young, "Development and application of GPS signal multipath simulator," *Radio Sci*, vol. 37, no. 6, 2002, doi: 10.1029/2001RS002549.

[8] S. Deep, S. Raghavendra, and B. D. Bharath, "GPS SNR prediction in urban environment," *Egyptian Journal of Remote Sensing and Space Science*, vol. 21, no. 1, 2018, doi: 10.1016/j.ejrs.2016.09.002.

[9] J. Lee, J. Seo, Y. S. Park, S. Pullen, and P. Enge, "Ionospheric threat mitigation by geometry screening in ground-based augmentation systems," *J Aircr*, 2011, doi: 10.2514/1.C031309.

This article has been accepted for publication in IEEE Transactions on Aerospace and Electronic Systems. This is the author's version which has not been fully edited and content may change prior to final publication. Citation information: DOI 10.1109/TAES.2023.3326134

[10] H. Lee, S. Pullen, J. Lee, B. Park, M. Yoon, and J. Seo, "Optimal Parameter Inflation to Enhance the Availability of Single-Frequency GBAS for Intelligent Air Transportation," *IEEE Transactions on Intelligent Transportation Systems*, vol. 23, no. 10, 2022, doi: 10.1109/TITS.2022.3157138.

[11] L. Marini-Pereira, S. Pullen, A. de O. Moraes, and J. Sousasantos, "Ground-Based Augmentation Systems Operation in Low Latitudes - Part 1: Challenges, Mitigations, and Future Prospects," *Journal of Aerospace Technology and Management*, vol. 13, 2021, doi: 10.1590/jatm.v13.1236.

[12] V. A. S. Pereira, J. F. G. Monico, and P. de O. Camargo, "Estimation and analysis of protection levels for precise approach at Rio De Janero international airport using real time σvig for each GPS and GLONASS satellite," *Boletim de Ciências Geodésicas*, vol. 27, no. spe, 2021, doi: 10.1590/s1982-21702021000s00010.

[13] J. Hu, Q. Sun, and X. Shi, "Multiple Reference Consistency Check Algorithm in GBAS Based on S-Values Auxiliary," in *Chinese Control Conference, CCC*, 2018. doi: 10.23919/ChiCC.2018.8483482.

[14] W. da Costa Silva and J. F. G. Monico, "GBAS: fundamentals and availability analysis according to σvig," *Journal of Geodetic Science*, vol. 12, no. 1, pp. 22–37, 2022, doi: 10.1515/jogs-2022-0132.

[15] R. Hatch, "The synergism of GPS code and carrier measurements," in *International geodetic symposium on satellite doppler positioning*, 1983, pp. 1213–1231.

[16] ICAO, "International Standards and Recommended Practices," in *Aeronautical Telecommunications, Annex 10 to the Convention of International Civil Aviation*, 2014.

[17] J. Budtho, P. Supnithi, and S. Saito, "Single-Frequency Time-Step Ionospheric Delay Gradient Estimation at Low-Latitude Stations," *IEEE Access*, vol. 8, 2020, doi: 10.1109/ACCESS.2020.3035247.

[18] S. Fujita, T. Yoshihara, and S. Saito, "Determination of ionosphere gradient in short baselines by using single frequency measurements," *Journal of Aeronautics, Astronautics and Aviation, Series A*, vol. 42, no. 4, pp. 269–276, 2010, [Online]. Available: http://www.scopus.com/inward/record.url?eid=2-s2.0-79851504297&partnerID=tZOtx3y1

[19] G. C. Ii, I. I. I. Sarps, N. S. Panel, N. S. P. W. Group, and N. Sarps, "Explanatory note GBAS CAT II / III Development Baseline SARPs," *Aids*, no. May, 2010.

[20] H. O. Hoffmann and R. O. Walton, "Integration of the ground-based augmentation system in continuous descent operations," *Navigation, Journal of the Institute of Navigation*, vol. 65, no. 4, 2018, doi: 10.1002/navi.262.

[21] M. Malinowski and J. Kwiecień, "A comparative study of precise point positioning (PPP) accuracy using online services," *Reports on Geodesy and Geoinformatics*, 2017, doi: 10.1515/rgg-2016-0025.

[22] Y. Mireault, P. Tétreault, F. Lahaye, P. Héroux, and J. Kouba, "Online precise point positioning: A new, timely service from natural resources Canada," *GPS World*, 2008.

[23] R. H. Mitch *et al.*, "Signal characteristics of civil GPS jammers," in *24th International Technical Meeting of the Satellite Division of the Institute of Navigation 2011, ION GNSS 2011*, 2011.

[24] K. Thanakan, K. Sapphaniran, T. Palasarn, P. Supnithi, W. Phakphisut, and C. Sakorn, "Real-time jamming detection and position estimation via software-defined radio (SDR)," in *ECTI-CON 2021 - 2021 18th International Conference on Electrical Engineering/Electronics, Computer, Telecommunications and Information Technology: Smart Electrical System and Technology, Proceedings*, 2021. doi: 10.1109/ECTI-CON51831.2021.9454678.

[25] Y. W. Lin, Y. T. Sung, S. J. Yeh, and S. S. Jan, "Flight test validation of ground based augmentation system prototype in Taiwan," in *Proceedings of the 33rd International Technical Meeting of the Satellite Division of the Institute of Navigation, ION GNSS+ 2020*, 2020. doi: 10.33012/2020.17581.

[26] J. Kadeřábek, V. Shapoval, P. Matějka, M. Kroulík, and F. Kumhála, "Comparison of four rtk receivers operating in the static and dynamic modes using measurement robotic arm," *Sensors*, vol. 21, no. 23, 2021, doi: 10.3390/s21237794.

JIRAPOOM BUDTHO received the B.E. and M.E. degrees in Telecommunication Engineering and Ph.D. in Electrical Engineering from King Mongkut's Institute of Technology Ladkrabang, Bangkok, Thailand, in 2015, 2017 and 2023, respectively. He is currently a lecturer with Telecommunication Engineering Department, School of Engineering, King Mongkut's Institute of Technology Ladkrabang, Thailand.

His research interests include the ionosphere, GBAS technology, GNSS, and Space Weather Information. He is also a member of Thai GNSS and the Space Weather Information Data Center.

PORNCHAI SUPNITHI (Senior Member, IEEE) received the B.S. degree from the University of Rochester, Rochester, NY, USA, in 1995, the M.S. degree from the University of Southern California, Los Angeles, CA, USA, in 1997, and the Ph.D. degree in electrical engineering from the Georgia Institute of Technology, Atlanta, GA, USA, in 2002.

In 2015, he became a Full Professor with Telecommunication Engineering Department, Faculty of Engineering, King Mongkut's Institute of Technology Ladkrabang. He has published over 50 journal articles, 100 conference papers, and three book chapters. His research interests include telecommunications, ionospheric and GNSS, data storage, and engineering education. His laboratory maintains numerous observation stations in Thailand (with ionosonde, beacon receivers, magnetometer, and GNSS receivers) and Thai GNSS and Space Weather information website (http://iono-gnss.kmitl.ac.th).

Prof. Dr. Supnithi currently serves as a Subcommittee Member of the National Research Council of Thailand (NRCT), the International Reference Ionosphere (IRI) Committee (under URSI, COSPAR), and the National GNSS Infrastructure Subcommittee, Ministry of Science and Technology, Thailand. He was a mid-career Thailand Research Fund Scholar, from 2013 to 2015. He has served as the second Vice President of the ECTI Association.

NATTAPONG SIANSAWASDI received the B.S. and M.S. degrees in telecommunication engineering from the Kasetsart University, Bangkok, Thailand, in 2002 and 2006, respectively. He is currently an air traffic system engineer at Air Traffic Navigation Systems Engineer Department, Aeronautical Radio of Thailand Ltd., Thailand.

His research interests include the ionospheric effects on GNSS, development of GNSS ground-based augmentation system.

SUSUMU SAITO received the B.S. degree in physics and the M.S. and Ph.D. degrees in ionospheric physics from Nagoya University, Japan, in 1995, 1997, and 2001, respectively. He is currently a Principal Researcher with the Electronic Navigation Research Institute, National Institute of Maritime, Port, and Aviation Technology, Tokyo, Japan. His current research interests include ionospheric effects on GNSS, development of GNSS ground-based augmentation system suitable for the low-latitude region, and ionospheric sciences using radio and optical techniques.

APITEP SAEKOW received the B.E. degree in computer and information from the Toyohashi University of Technology, Japan, in 1996, the M.S. degree in computer science from La Trobe University, Australia, in 1998, and the Ph.D. degree in computer engineering from the Thammasat University, Thailand, in 2010.

He has over 18 years of experience in teaching in Japan, Australia and Thailand and five years working as a dean and an assistant president for various key roles: academic affairs, academic services and external affairs and International Relations at Stamford International University. He is also a government consultant and a researcher in e-Government interoperability projects. His research interests are Interoperability in e-Government, e-Business, e-Commerce, Research Methodology, Artificial Intelligence, Genetic Algorithms and Education Management.

He was a researcher of the winner project of e-Asia Award in India. In 2014, he won the Blackboard Catalyst Award on Innovative Blended Learning from US in 2016. Since 2019, he has served as the Acting President at Stamford International University, Thailand.

LIN M. M. MYINT received the B.E. degree in electronics from the Assumption University, Thailand, in 2001, the M.E. degree in telecommunications from the Asian Institute of Technology, Thailand, in 2003, and the Ph.D. degree in IT from the Shinawatra University, Thailand, in 2011. He is currently an Assistant Professor with the King Mongkut's Institute of Technology Ladkrabang, Thailand. He is a member of Thai GNSS and the Space Weather Information Data Center.

His research interests include signal processing on data storage and communications, space weather analysis, and GNSS positioning and navigation.